Supplementary Figures

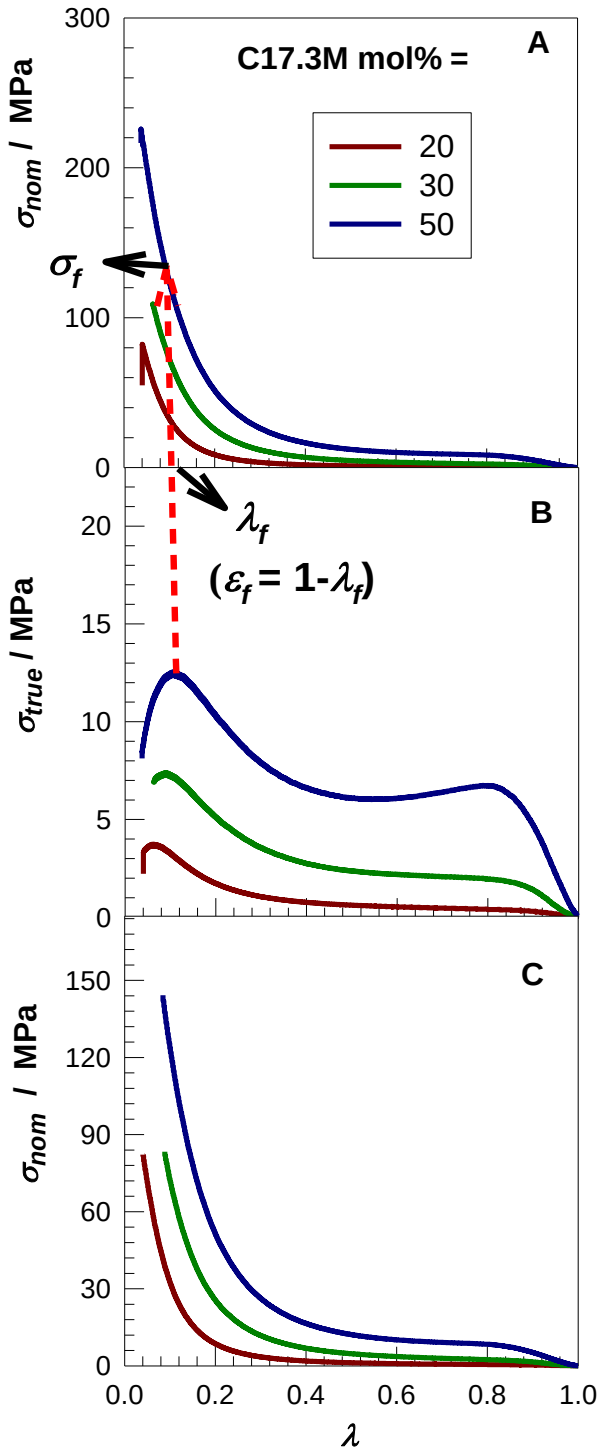

Figure S1. Typical stress-strain curves of DMA/C17.3M hydrogels under compression as the dependences of the nominal σ_{nom} (A) and true stresses σ_{true} (B) on the compression ratio λ. The dashed red arrow illustrates calculation of the real fracture stress for the hydrogel containing 50 mol% C17.3M from the maximum in σ_{true} vs λ curve. The corrected σ_{nom} *vs* λ curves up to the fracture point are shown in C.

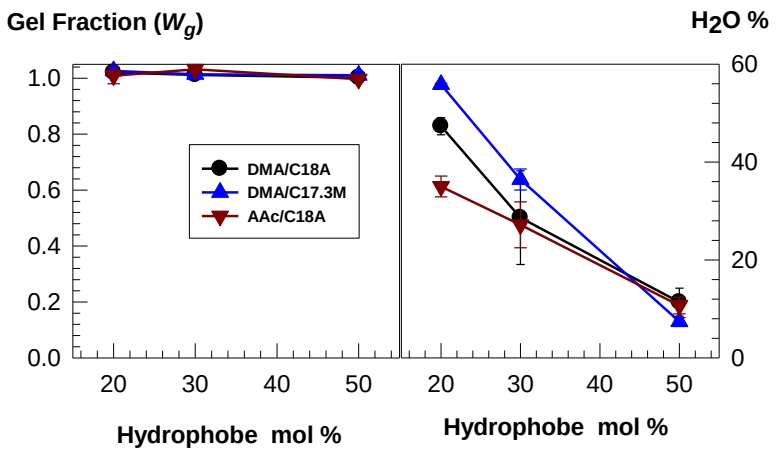

Fig. S2. Gel fraction W_g and equilibrium water content (H_2O %) of the hydrogels plotted against their hydrophobe content.

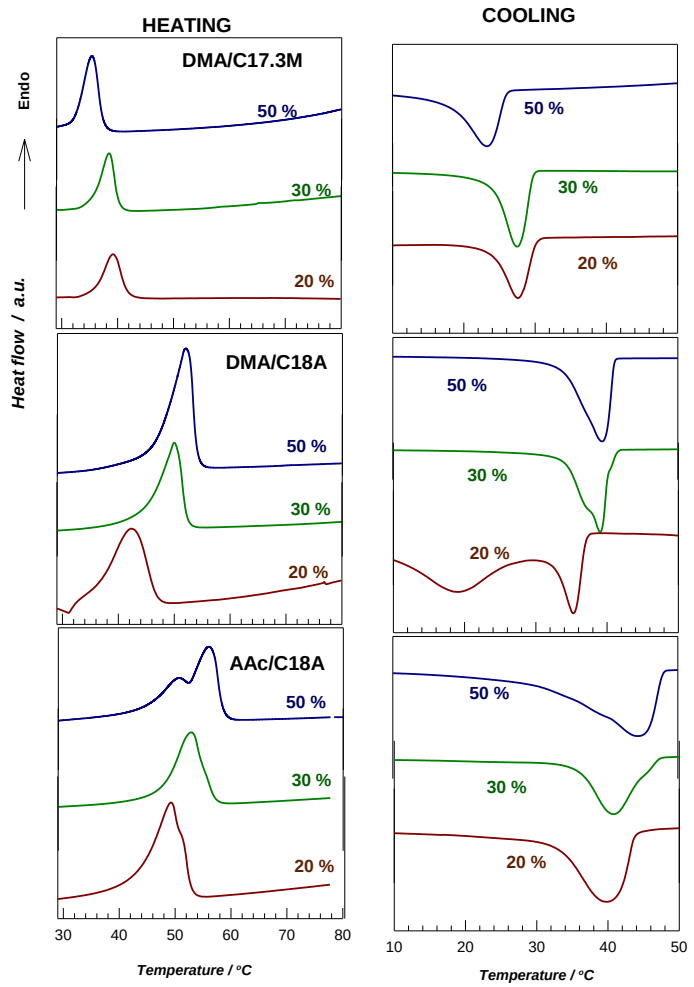

Fig. S3. DSC traces of the hydrogels. The type of the hydrogels and their hydrophobe content are indicated.

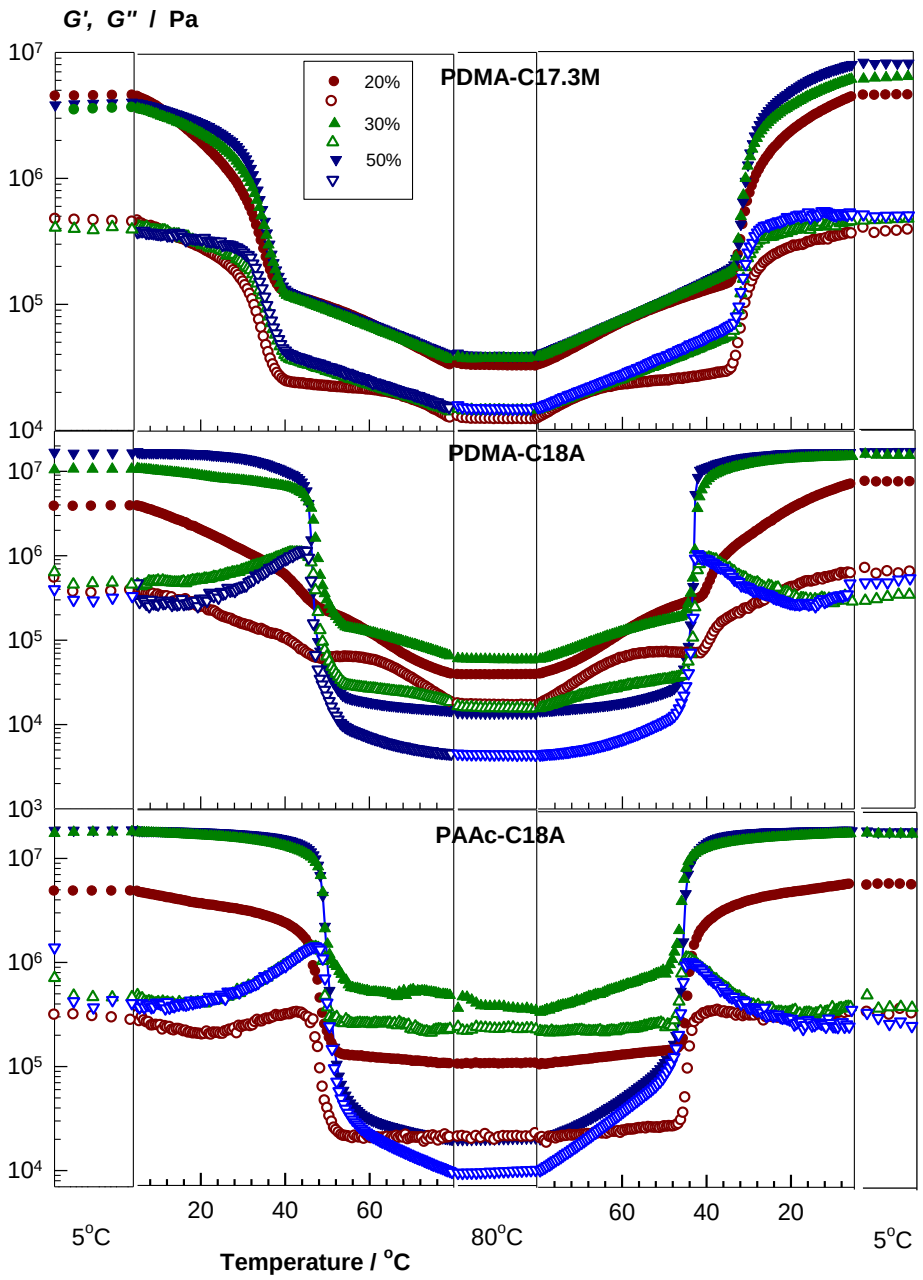

Fig. S4. *G'* (filled symbols), and *G''* (open symbols) of the hydrogels during the heating - cooling cycle between 5 and 80 °C. The type of the hydrogels and their hydrophobe content indicated. $\omega = 6.28$ rad.s^{-1}. $\gamma_0 = 0.001$.

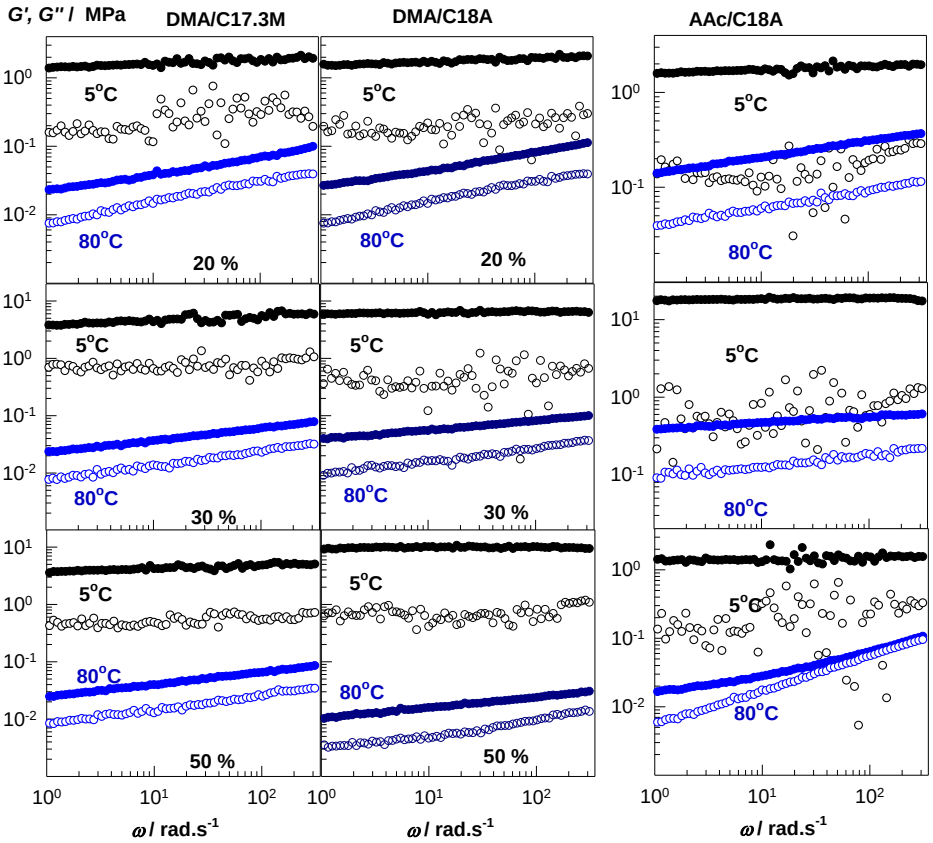

Fig. S5 *G'* (filled symbols) and *G''* (open symbols) of the hydrogels with 20, 30, and 50 mol% hydrophobe at 5 and 80 °C shown as a function of the frequency ω. $\gamma_0 = 0.001$.

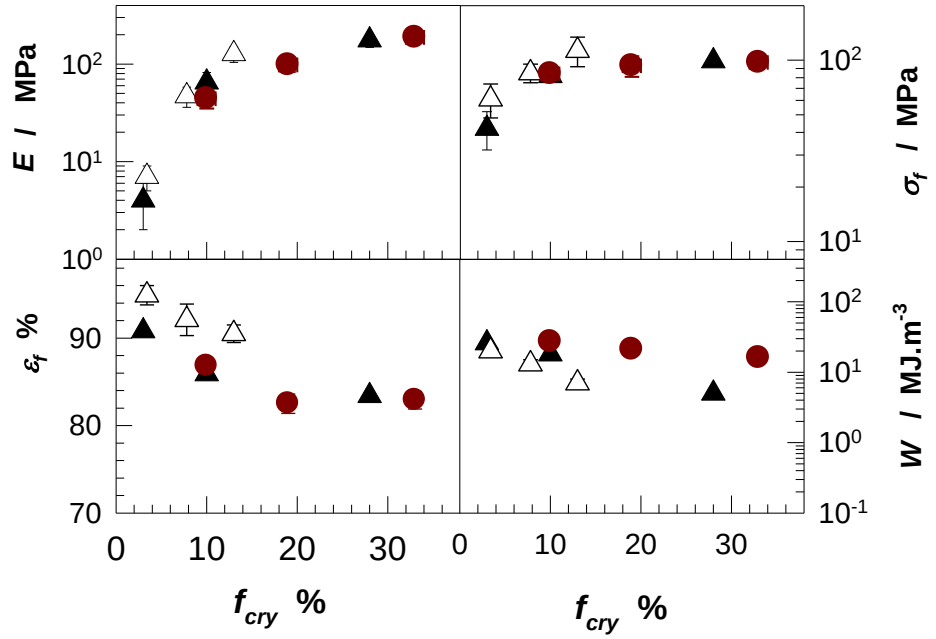

Fig. S6. Young's modulus E, compressive fracture stress σ_f, fracture strain ε_f, and toughness W of the hydrogels plotted against the fraction f_{cry} of units in crystalline domains. Hydrogels: DMA/C17.3M (△), DMA/C18A (▲), AAc/C18A (●).

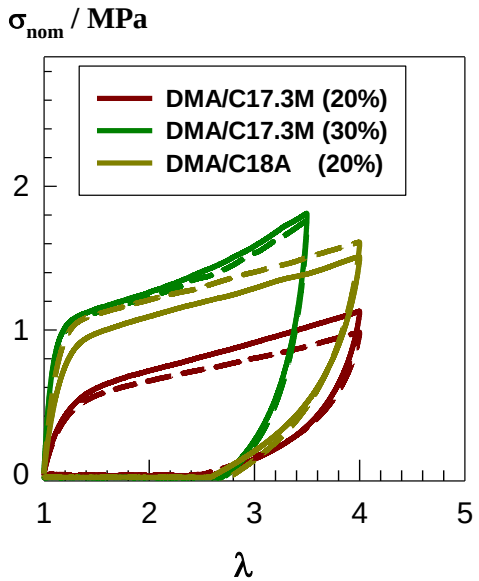

Figure S7. (A): Two successive loading / unloading tensile cycles up a maximum elongation ratio λ_{max} of 3.5 and 4.0 for the hydrogel samples indicated. Note that between each cycle, the gel samples were immersed in water at 70 °C. 1st and 2nd cycles are shown by the solid and dashed curves, respectively.